DOI: 10.1021/cg901582j

CRYSTAL GROWTH & DESIGN Article

2010, Vol. 10
2267–2271

# Microcrystals Electrodeposited in a High Magnetic Field

Anne-Lise Daltin* and Jean-Paul Chopart

*LACM-DTI, LRC CEA, Université de Reims Champagne-Ardenne, B.P. 1039, 51687 Reims Cedex 2, France*

*Received December 16, 2009; Revised Manuscript Received February 5, 2010*

**ABSTRACT:** The growth of $Cu_2O$ crystallites electrodeposited in a nitrate bath with sodium dodecyl sulfate (SDS) under superimposition of a high magnetic field up to 12 T was investigated. Scanning electron micrographs show that the morphology of the crystallite changes from a starlike shape to a well-faceted octahedron with magnetohydrodynamic (MHD) convection. The magnetic field modifies the branching growth of $Cu_2O$ microcrystals.

## Introduction

There is increasing attention on the shape-controlled synthesis of cuprous oxide micro- and nanocrystals due to the fact that morphology and size play very important roles in enhancing the desired properties and stabilities.[1−11] $Cu_2O$ has been synthesized in several shapes, such as sphere,[12−14] octahedron,[15] nanowire,[16−24] hollow sphere, polyhedron and cube,[6,7,25−27] nanodot,[28,29] hexapodlike whisker,[30] and multipod framework.[4] Cuprous oxide is a brick-red, p-type semiconductor with a band gap of about 2.2 eV.[31,32] $Cu_2O$ deposits are nontoxic and suitable for numerous applications, such as in photovoltaic devices, and are used in conversion of optical, electrical, and chemical energy. The shape and size of this material are well-known to have great effects on their properties and corresponding potential applications. For example, the optical absorption would be affected considerably by the morphology and crystallinity of $Cu_2O$ crystals.[15] Xu et al. have shown that $Cu_2O$ octahedrons with exposed {111} crystal surfaces possess much higher activity than cubes.[33] Such investigations may provide guidance for the shape-controlled synthesis of $Cu_2O$ crystals with tunable size and their application in the treatment of organic pollutants. Recently, a novel nonenzymatic sensor made of porous $Cu_2O$/Nf on a glass carbon electrode has been prepared.[34] The experimental investigations have shown that porous $Cu_2O$ microcubes provide abundant active sites for sensing of $H_2O_2$ and glucose.

Deposition of this inorganic material by an electrochemical technique from aqueous solutions has attracted much research interest because it is an inexpensive and convenient method. Siegfried and co-workers[8,9] have studied an electrochemical growth route to obtain $Cu_2O$ microcrystals with a vast array of architectures and display parameters that can systematically control branching or faceting growth. A common method to manipulate crystal habit is to employ a growth medium containing additives that can preferentially adsorb on specific crystallographic planes. This method changes the direction and rate of crystal growth and results in crystals with different final morphologies.

When a magnetic field is applied onto an electrochemical cell parallel to the electrode surface, some forces can create flux along the electrode. Most experimental works deal with a constant and uniform magnetic field parallel to the plane substrate; in this case, the Lorentz force $\vec{j} \times \vec{B}$ is involved. When the magnetic field lines are perpendicular to the substrate and therefore parallel to the current lines, a so-called paramagnetic force can be efficient if paramagnetic species are under mass transport control.[35−37] These forces induce convective effects, modify alloy composition and surface smoothness, and could generate modification of morphology and texture of metals, alloys (ref 38 and references therein), and oxide.[39]

Microconvective phenomena inside the diffusion layer could be induced. These effects are possible not only in ferromagnetic materials but also in nonmagnetic ones such as paramagnetic materials. The magnetic force effect on paramagnetic species has been analyzed.[36] Some papers have reported that convective effects are created by a magnetic field perpendicular to the surface of a plane electrode when the involved species are paramagnetic and a diffusion limiting current dependence on both the gradient concentration species and the magnetic field amplitude has been claimed.[37] Moreover, in the presence of inhibiting species, the textural and morphological changes generated by a magnetic field could be provoked by the increase of the diffusion flux of these definite inhibiting species toward the cathode.[40] However, the influence of a high magnetic field on the tunable morphology of cuprous oxide has not yet been reported.

In this study we have explored the influence of a high magnetic field on the stability and growth of various crystallographic planes of growing $Cu_2O$ crystals. Herein the electroactive ($Cu^{2+}$) paramagnetic ions are involved (molar magnetic susceptibilities $\chi_m = 16.10^{-9}$ $m^3$/mol). Electrodeposition of $Cu_2O$ has been undertaken in a galvanostatic mode on austenitic 304 stainless steel.

## 2. Experimental Section

Cuprous oxide ($Cu_2O$) crystals were prepared from an aqueous electrolytic bath containing 0.02 M $Cu(NO_3)_2 \cdot 3H_2O$ using an electrodeposition method; 0.17 M $NaC_{12}H_{25}O_4S$ (SDS) was used as surfactant agent. All the chemical reagents used in this experiment were analytical grade. The pH of the electrolytic solution was equal to 5.6 with SDS. Polycrystalline austenitic 304 stainless steel was used as substrate. Before substrates (surface area 1 $cm^2$) were used in the electrolytic bath, they were polished with Struers paper down to 4000 mesh and cleaned with distilled water.

$Cu_2O$ particles have been deposited in a galvanostatic mode at 60 °C for various times. Experiments have been performed with a

*To whom correspondence should be addressed. E-mail: al.daltin@univ-reims.fr. Telephone: +33 3 26 91 84 49. Fax: +33 3 26 91 89 15.



Published on Web 02/25/2010

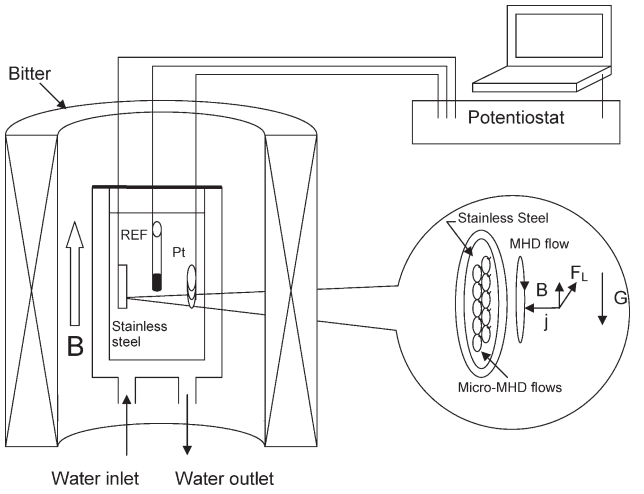


**Figure 1.** Schematic view of the experimental apparatus for electrodeposition under high magnetic field.

classical three-electrode cell that was thermostatically controlled. The electrolytic cell (100 $cm^3$) was put into the gap of a Bitter Magnet (130 mm diameter bore, 12 MW, available at the CNRS National High Magnetic Field Laboratory in Grenoble). The applied magnetic field was considered as uniform and homogeneous ($\Delta B/B = 100 \times 10^{-6}$) onto the whole cell. Vertical magnetic fields up to 12 T being parallel to the electrode surface have been generated during experiments. The experiments were achieved using a potentiostat−galvanostat PGZ 301 (Tacussel-Radiometer Inc., Copenhagen). All electrodepositions were carried out with a current density equal to 70 $\mu A \cdot cm^{-2}$. Figure 1 shows the schematic view of the experimental apparatus.

The X-ray diffraction (XRD) study of deposits was carried out in the range of the scanning angle 20−80° with Cu Kα ($\lambda = 0.15406$ nm) using a BRUKER D8 ADVANCE X-ray diffractometer. The microstructure was studied using a scanning electron microscope (SEM) (model JEOL JSM 6460LA) attached with an EDS JEOL 1300 microprobe.

## 3. Results and Discussion

Figure 2a and d shows the results of electrochemical deposition during 10 and 20 min without a magnetic field on a stainless steel substrate. They indicate that, with surfactant agent and without magnetic field, the crystal habit is octahedral and that 6-pod branching growth along the ⟨100⟩ direction is observed. Crystals grow up with time, but we do not observe an increase of the number of crystallites, and there is no new nucleation of crystallites between the observation after 10 min and the one after 20 min. Under a superimposition of a 6 T magnetic field (Figure 2b and e), it was found that the morphology has evolved. In such a case, some crystals have branching growth, and some others do not have. These ultimate crystallites have homogeneous octahedral shape. When a high magnetic field of 12 T was superimposed on the electrochemical cell (Figure 2c and f), the cuprous oxide exhibits a very regular octahedral shape with the {111} faces maintained in the final appearance. The number density of observable crystallites is enhanced with B, as can be seen in Figure 2a, b, and c for respectively 0, 6, and 12 T. In all cases, the crystal habit is octahedral even if the morphology evolves with magnetic field. In previous work, Siegfried and co-workers[41] indicated that when SDS is added to the electrolyte, the crystal habit changes from cubic to octahedral. The preferential adsorption of SDS onto the {111} faces hinders crystal growth along the ⟨111⟩ direction. So, faster growing {100} facets are eliminated in the final morphology forming octahedral shapes.

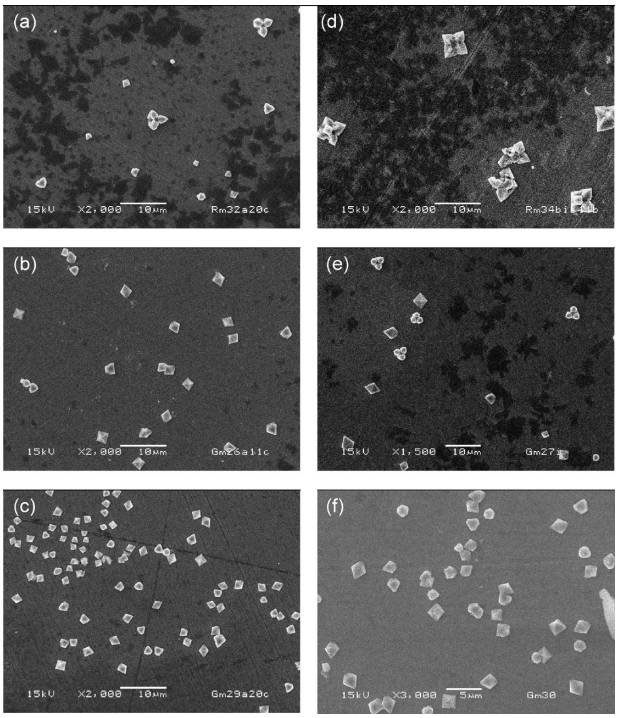


**Figure 2.** SEM images of $Cu_2O$ crystallites electrodeposited in a nitrate bath with SDS with $B = 0$ T (a, d), $B = 6$ T (b, e), and $B = 12$ T (c, f), respectively; $t = 10$ min (a−c) or $t = 20$ min (d−f); $I = 70\ \mu A \cdot cm^{-2}$.

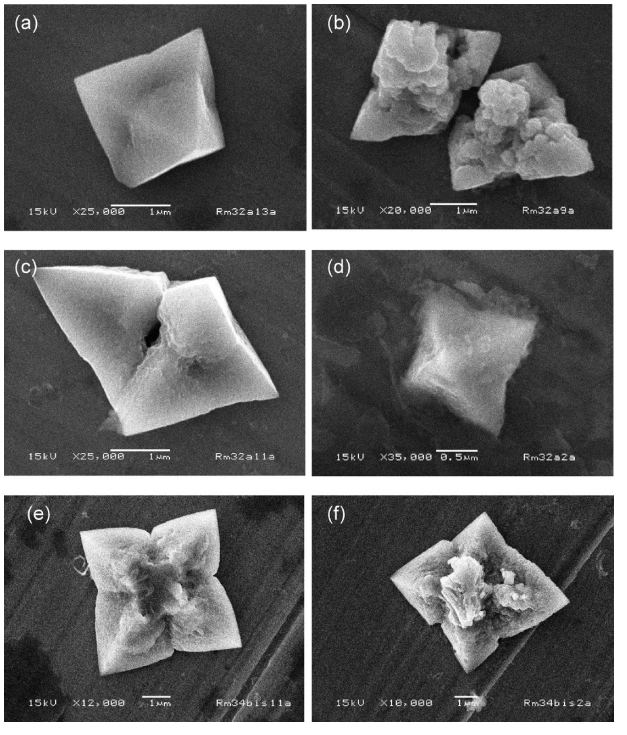


**Figure 3.** SEM images of $Cu_2O$ isolated crystallite electrodeposited in a nitrate bath with SDS without B; $t = 10$ min (a−d) and $t = 20$ min (e and f); $I = 70\ \mu A \cdot cm^{-2}$.

Parts a−d of Figure 3a−d are high magnification micrographs of crystallites electrodeposited for 10 min without a magnetic field. The average size of these crystallites is about a few micrometers. Starlike particles derived from six edge-sharing octahedral units with some deformation of the primary

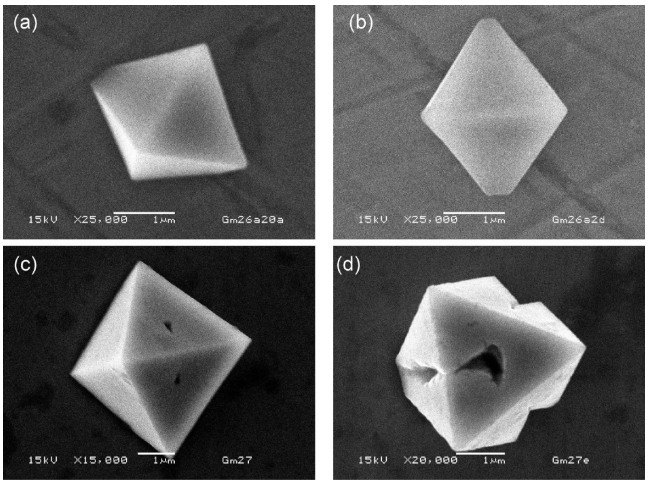


**Figure 4.** SEM images of $Cu_2O$ isolated crystallite electrodeposited in a nitrate bath with SDS with $B = 6$ T; $t = 10$ min (a and b) and $t = 20$ min (c and d); $I = 70\ \mu A \cdot cm^{-2}$.

crystals are observed. Mesophase crystals can become truncated by the substrate for certain orientations. On the right top image in Figure 3b, it can be seen that the starlike particles are in fact the assembly of nanoscopic polyhedral single crystals. The particles shown in Figure 3e and f, obtained at 0 T for a 20-min deposition, have a truncated star-shaped morphology and are bigger than those observed for an electrodeposition time equal to 10 min. When a 6 T magnetic field is applied during 10 min, well-defined octahedra are synthesized (Figure 4a and b). The lengths of the octahedral crystal sides are up to 2.2 $\mu$m. In Figure 4c and d, crystal aggregates can be highlighted. These microcrystals are packed in a simple octahedron lattice showing an octahedron-within-octahedron arrangement. The presence of porosity in the center of each three octahedral unit pack is revealed for microcrystals electrodeposited with a 6 T magnetic field during 20 min. Therefore, eight emerging holes are assumed to be present in the octahedral arrangement that is composed by six octahedra which form one hexapod. With increasing magnetic field, a higher magnification image reveals that the particles have an octahedral shape with a side length between ~1 and 2 $\mu$m (Figure 5).

The X-ray diffraction (XRD) patterns of the samples prepared with or without superimposition of a magnetic field have been obtained. The major peaks located at $2\theta$ values of 20° to 80° correspond for all cases to the characteristic diffraction patterns of cubic phase $Cu_2O$ (JCPDS, 05-0667). No peak of Cu or CuO appears. Parts of the X-ray diffraction patterns of crystals electrodeposited from the nitrate bath with SDS under $B = 0$ and 12 T are shown in Figure 6 a and b, for $2\theta$ values included between 28° and 43°. The relative intensities of (110), (111), and (200) reflections provide information regarding the crystal orientation against the substrate. A very high (111) peak is present without any other orientation in the case of a 12 T magnetic field. That means that most of the octahedra form interfaces with the substrate using the {111} planes. Without a magnetic field, a (200) peak and a (111) smaller one are observed which confirm the different orientations of crystals on the stainless steel substrates revealed by SEM analyses.

In fact, under high magnetic field (12 T), only simple (1−2 $\mu$m side size) octahedra without any arrangement are obtained and are preferentially oriented on the substrate with {111} faces parallel to the substrate. Under a 6 T intermediate

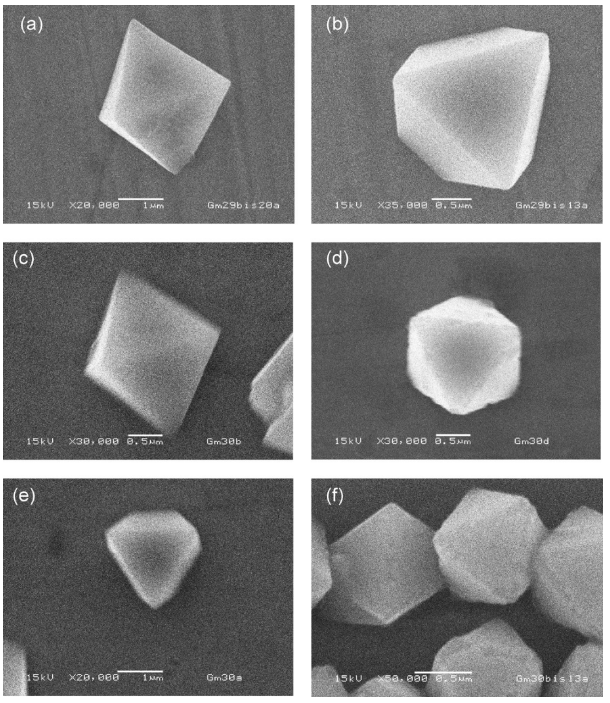


**Figure 5.** SEM images of $Cu_2O$ isolated crystallite electrodeposited in a nitrate bath with SDS with $B = 12$ T. $t = 10$ min (a and b) and $t = 20$ min (c−f); $I = 70\ \mu A \cdot cm^{-2}$.

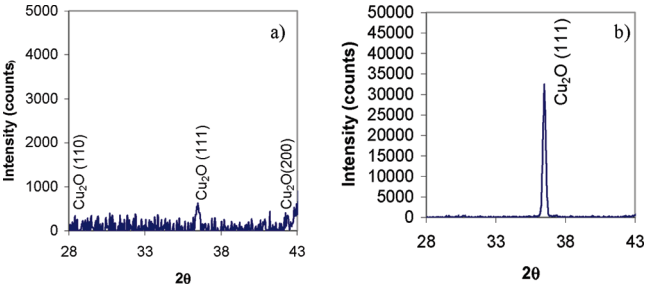


**Figure 6.** X-ray diffraction of the crystallites: (a) $B = 0$ T, $t = 20$ min, $I = 70\ \mu A \cdot cm^{-2}$; (b) $B = 12$ T, $t = 20$ min, $I = 70\ \mu A \cdot cm^{-2}$.

magnetic field, no arrangement is seen after a 10-min electrodeposition, but arrangement of bigger crystals with intracrystal porosity partially eliminated has been obtained after 20 min. Finally, without a magnetic field, there is always an arrangement of six-subunit octahedron crystals that form starlike particles.

When a magnetic field couples with the bended electric force lines, a complex microscopic convection, "micro-MHD" is generated. With a magnetic field parallel to the substrate, due to the complex morphology of the crystallites, all the magnetic forces mentioned above (Lorentz and paramagnetic forces) can be involved. The crystal growth morphology is directly related to internal and external habit-controlling factors which depend on the structure of the interface, the composition of the system, and other parameters affecting the growth process such as the above-mentioned microconvection induced by the magnetic field.

In Figure 2a, crystallites with different sizes are observed while, in Figure 2c, a more homogeneous distribution of crystallite sizes is obtained. In our experiments with or without a magnetic field, the number density of active sites could not be very different because it depends on the substrate

pretreatment and on the applied potential. The former one has always been carried out in the same way, and the second one was constant in all cases: only a difference equal to 5 mV for the electrode potential has been noticed during these depositions. Figure 2d and f indicates an increase of the crystallite number with smaller crystallites when the deposition process is undertaken with a superimposed magnetic field, and it is obvious (Figure 2c and f) that high magnetic field produces a similar growth for each nucleus.

A larger number of smaller crystallites induces a bigger real integral active surface area of $Cu_2O$ while the total volume of oxide deposit is not changed because it is only determined by the current density and the total deposition time.

Apparently the above results and these hypotheses suggest that the superimposition of the magnetic field induces an increase of the growth rate along the ⟨100⟩ directions.

As reported by Choi,[42] the formation of $Cu_2O$ is attributed to the reduction of $Cu^{2+}$ ions to $Cu^+$ ions (eq 1),

$$Cu^{2+} + e^- \rightarrow Cu^+ \quad (1)$$

followed by precipitation of $Cu_2O$ due to the low solubility of $Cu^+$ ions

$$2Cu^+ + H_2O \rightarrow Cu_2O + 2H^+ \quad (2)$$

Due to the low concentration of $Cu^{2+}$ species, it can be assumed that the mechanism is under mass transport control; Cu(II) and hydronium species diffuse respectively toward the electrode and toward the bulk of the solution. The magnetic field generates convection that enhances the diffusion rate of Cu(II) ions which arrive on the surface of $Cu_2O$ and the diffusion rate of $H^+$ ions that leave the surface (retrodiffusion). This convection inhibits the local decrease of pH due to the reaction presented in eq 2. In fact, the magnetic field via the magnetic forces homogenizes the solution near the surface of the electrodeposited crystallites, there is less depletion of copper ions near the $Cu_2O$ surface, and therefore, the magnetic field increases the current density on each nucleus from the very beginning of the growth process[43] and, therefore, increases the number of the nuclei which can be observed.

The more important adsorption of SDS on the nonpolar {111} faces (while {100} surfaces are polar in the $Cu_2O$ crystal because of the succession of cationic $Cu^+$ and anionic $O^{2-}$ layers) lowers the surface energy of the bound plane and hinders the crystal growth along the ⟨111⟩ direction. It has been highlighted that the adsorption of SDS was most effective for higher pH. The above mechanism of $Cu_2O$ formation leads to a decrease of the local pH and therefore to a decrease of the efficiency in SDS adsorption; the magnetically induced convection provokes a retrodiffusion of the protons that are formed during the electrodeposition process and so limits the decrease of the pH at the surface of the deposit; this fact results in an octahedral shape modification in adsorption of SDS during the electrodeposition process under MHD that allows a selective growth rate of $Cu_2O$ crystals along the ⟨111⟩ directions and, therefore, leads to their final morphology.

## 4. Conclusion

With SDS in the electrolytic bath, a superimposed magnetic field generates faceted shapes. On the other hand, in the same case without MHD, branching growth is allowed due to the competition between the promotion and reduction of crystal growth, connected with species diffusion effects (concentration more important on the edges of the crystals than in the center of faces). The change from starlike shape to well-faceted smaller octahedron is attributed to a decrease of the influence of $Cu^{2+}$ species diffusion on the crystal growth linked with SDS adsorption.

A basic crystal shape is determined by two growth processes: habit formation (thermodynamic control) and branching growth (kinetic control). Surface energy is minimized during growth. So the external faces are the lowest energy faces. One can assume that magnetic field acts principally on branching growth that is generated by the convection phenomena acting on the diffusive species. Edges, more concentrated in species, grow faster than the centers of faces.

In the case of cuprous oxide electrodeposition, the superimposition of magnetic field induced a significant change in crystal morphology. This branching growth enhancement could be caused by macroscopic or microscopic MHD convections.

**Acknowledgment.** This work was financially supported by the Champagne-Ardenne Council and the European Community through Program No. RITA-CT-2003-505474. The authors want to thank the LNCMI team in Grenoble for helpful assistance. This study has been performed in the frame of GDRE GAMAS.

## References

(1) Dong, Y.; Li, Y.; Wang, C.; Cui, A.; Deng, Z. *J. Colloïd Interface Sci.* **2001**, *243*, 85–89.
(2) Wang, W.; Wang, G.; Wang, X.; Zhan, Y.; Liu, Y.; Zheng, C. *Adv. Mater.* **2002**, *14* (1), 67–69.
(3) Wang, W.; Varghese, O. K.; Ruan, C.; Paulose, M.; Grimes, C. A. *J. Mater. Res.* **2003**, *18* (12), 2756–2759.
(4) Chang, Y.; Zeng, H. C. *Cryst. Growth Des.* **2004**, *4* (2), 273–278.
(5) Wu, Y.; Livneh, T.; Zhang, Y. X.; Cheng, G.; Wang, J.; Tang, J.; Moskovits, M.; Stucky, G. D. *Nanoletters* **2004**, *4* (12), 2337–2347.
(6) Luo, F.; Wu, D.; Gao, L.; Lian, S.; Wang, E.; Kang, Z.; Lan, Y.; Xu, L. *J. Cryst. Growth* **2005**, *285*, 534–540.
(7) Chang, Y.; Teo, J. J.; Zeng, H. C. *Langmuir* **2005**, *21*, 1074–1079.
(8) Siegfried, M. J.; Choi, K. S. *Angew. Chem., Int. Ed.* **2005**, *44*, 3218–3223.
(9) Siegfried, M. J.; Choi, K. S. *J. Am. Chem. Soc.* **2006**, *128*, 10356–10357.
(10) Li, H.; Liu, R.; Zhao, R.; Zheng, Y.; Chen, W.; Xu, Z. *Cryst. Growth Des.* **2006**, *6* (12), 2795–2798.
(11) Singh, D. P.; Neti, N. R.; Sinha, A. S. K.; Srivastava, O. N. *J. Phys. Chem. C* **2007**, *111*, 1638–1645.
(12) Muramatsu, A.; Sugimoto, T. *J.Colloïd Interface Sci.* **1997**, *189* (1), 167–173.
(13) Yang, H.; Ouyang, J.; Tang, A.; Xiao, Y.; Li, X.; Dong, X.; Yu, Y. *Mater. Res. Bull.* **2006**, *41*, 1310–1318.
(14) Zhang, J.; Liu, J.; Peng, Q.; Wang, X.; Li, Y. *Chem. Mater.* **2006**, *18*, 867–871.
(15) He, P.; Shen, X.; Gao, H. *J. Colloïd Interface Sci.* **2005**, *284*, 510–515.
(16) Schonenberger, C.; van der Zande, B. M. I.; Fokkink, L. G. J.; Henny, M.; Schmid, C.; Kruger, M.; Bachtold, A.; Huber, R.; Birk, H.; Staufer, U. *J. Phys. Chem. B* **1997**, *101*, 5497–5505.
(17) Huang, L.; Wang, H.; Wang, Z.; Mitra, A.; Zhao, D.; Yan, Y. *Chem. Mater.* **2002**, *14*, 876–880.
(18) Mei, Y. F.; Siu, G. G.; Yang, Y.; Fu, R. K.Y.; Hung, T. F.; Chu, P. K.; Wu, X. L. *Acta Material.* **2004**, *52*, 5051–5055.
(19) Daltin, A. L.; Addad, A.; Chopart, J. P. *J. Cryst. Growth* **2005**, *282*, 414–420.
(20) Han, S.; Chen, H. Y.; Chu, Y. B.; Shih, H. C. *J. Vac. Sci. Technol., B* **2005**, *23* (6), 2557–2560.
(21) Liu, X. M.; Zhou, Y. C. *Appl. Phys. A: Mater. Sci. Process.* **2005**, *81*, 685–689.
(22) Ko, E.; Choi, J.; Okamoto, K.; Tak, Y.; Lee, J. *Chem. Phys. Chem.* **2006**, *7*, 1505–1509.
(23) Das, K.; De, S. K. *J. Lumin.* **2009**, *129*, 1015–1022.

(24) Orel, Z. C.; Anzlovar, A.; Drazic, G.; Zigon, M. *Cryst. Growth Des.* **2007**, *7* (2), 453–458.
(25) Xu, L.; Chen, X.; Wu, Y.; Chen, C.; Li, W.; Pan, W.; Wang, Y. *Nanotechnology* **2006**, *17*, 1501–1505.
(26) Zhang, H.; Shen, C.; Chen, S.; Xu, Z.; Liu, F.; Li, J.; Gao, H. *Nanotechnology* **2005**, *16*, 267–272.
(27) Chen, M.; Diao, G.; Zhou, X. *Nanotechnology* **2007**, *18*, 275606 (10pp).
(28) Lyubinetsky, I.; Lea, A. S.; Thevuthasan, S.; Baer, D. R. *Surf. Sci.* **2005**, *589*, 120–128.
(29) Li, L.; Wang, J.; Wang, R.; Liu, H.; Jia, C.; Ma, L.; Yu, Y. *Appl. Phys. Lett.* **2006**, *89*, 113109-1–3.
(30) Chen, Z. Z.; Shi, E. W.; Zheng, Y. Q.; Ji, W.; Xiao, B.; Zhuang, J. Y. *J. Cryst. Growth* **2003**, 249–300.
(31) Ray, S. C. *Sol. Energy Mater. Sol. Cells* **2001**, *68*, 307–312.
(32) Ghijsen, J.; Tjeng, L. H.; van Elp, J.; Eskes, H.; Westerink, J.; Sawatzky, G. A.; Czyzyk, M. T. *Phys. Rev. B* **1988**, *38* (16), 11322–11330.
(33) Xu, H.; Wang, W.; Zhu, W. *J. Phys. Chem. B* **2006**, *110*, 13829–13834.
(34) Zhang, L.; Li, H.; Ni, Y.; Li, J.; Liao, K.; Zhao, G. *Electrochem. Commun.* **2009**, *11*, 812–815.
(35) O'Brien, R. N.; Santhanam, K. S. V. *J. Appl. Electrochem.* **1997**, *27*, 573–578.
(36) Leventis, N.; Gao, X. *J. Am. Chem. Soc.* **2002**, *124*, 1079–1088.
(37) Rabah, K. L.; Chopart, J. P.; Schloerb, H.; Saulnier, S.; Aaboubi, O.; Uhlemann, M.; Elmi, D.; Amblard, J. *J. Electroanal. Chem.* **2004**, *571*, 85.
(38) Alemany, A.; Chopart, J. P. In *Fluid Mechanics and its Application*; Molokov, S., Moreau, R., Moffatt, H. K., Eds.; Springer: Dordrecht, The Netherlands, 2007; Vol. 80, pp 391−407.
(39) Morisue, M.; Nambu, M.; Osaki, H.; Fukunaka, Y. *J. Solid State Electrochem.* **2007**, *11*, 719–726.
(40) Devos, O.; Aaboubi, O.; Chopart, J. P.; Merienne, E.; Olivier, A.; Amblard, J. *J. Electrochem. Soc.* **1998**, *145* (12), 4135–4139.
(41) Siegfried, M. J.; Choi, K. S. *Adv. Mater.* **2004**, *16* (19), 1743–1746.
(42) Choi, K. S. *Dalton Trans.* **2008**, 5432–5438.
(43) Daltin, A. L.; Bohr, F.; Chopart, J. P. *Electrochim. Acta* **2009**, *54*, 5813–5817.